Cell Reports

Report

Acute Complexin Knockout Abates Spontaneous and Evoked Transmitter Release

Graphical Abstract

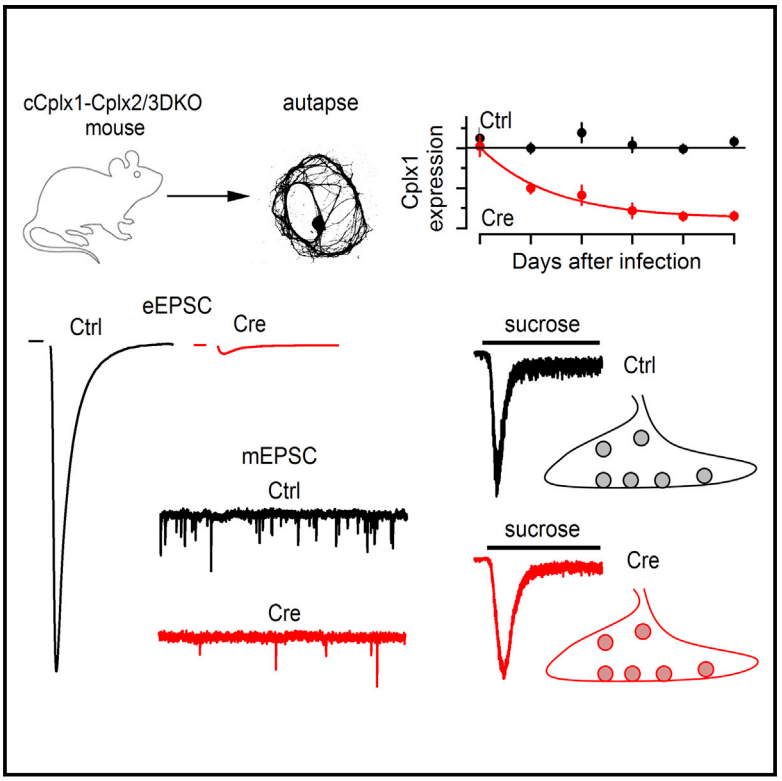

Authors

Francisco José López-Murcia, Kerstin Reim, Olaf Jahn, Holger Taschenberger, Nils Brose

Correspondence

htasche@gwdg.de (H.T.), brose@em.mpg.de (N.B.)

In Brief

Complexins are thought to either promote synaptic vesicle fusion or act as "fusion clamps." López-Murcia et al. show that acute genetic complexin deletion reduces the rates of all forms of transmitter release in forebrain neurons without affecting vesicle priming. Thus, complexins are facilitators of vesicle fusion and dispensable for "fusion clamping."

Highlights

- Conditional complexin (Cplx) 1 KO mouse forebrain neurons were generated
- Acute Cplx KO attenuates spontaneous, synchronous, asynchronous, and delayed SV fusion
- Acute Cplx KO does not cause "fusion unclamping" or affect vesicle priming
- Cplxs are facilitators of synaptic vesicle fusion and dispensable for "fusion clamping"

López-Murcia et al., 2019, Cell Reports *26*, 2521–2530
March 5, 2019
https://doi.org/10.1016/j.celrep.2019.02.030

CellPress

Cell Reports
Report

Acute Complexin Knockout Abates Spontaneous and Evoked Transmitter Release

Francisco José López-Murcia,[1,4] Kerstin Reim,[1,4] Olaf Jahn,[2,3] Holger Taschenberger,[1,3,*] and Nils Brose[1,3,5,*]
[1]Department of Molecular Neurobiology, Max Planck Institute of Experimental Medicine, 37075 Göttingen, Germany
[2]Proteomics Group, Max Planck Institute of Experimental Medicine, 37075 Göttingen, Germany
[3]DFG-Research Center for Nanoscale Microscopy and Molecular Physiology of the Brain, 37073 Göttingen, Germany
[4]These authors contributed equally
[5]Lead Contact
*Correspondence: htasche@gwdg.de (H.T.), brose@em.mpg.de (N.B.)
https://doi.org/10.1016/j.celrep.2019.02.030

SUMMARY

SNARE-mediated synaptic vesicle (SV) fusion is controlled by multiple regulatory proteins that determine neurotransmitter release efficiency. Complexins are essential SNARE regulators whose mode of action is unclear, as available evidence indicates positive SV fusion facilitation and negative "fusion clamp"-like activities, with the latter occurring only in certain contexts. Because these contradictory findings likely originate in part from different experimental perturbation strategies, we attempted to resolve them by examining a conditional complexin-knockout mouse line as the most stringent genetic perturbation model available. We found that acute complexin loss after synaptogenesis in autaptic and mass-cultured hippocampal neurons reduces SV fusion probability and thus abates the rates of spontaneous, synchronous, asynchronous, and delayed transmitter release but does not affect SV priming or cause "unclamping" of spontaneous SV fusion. Thus, complexins act as facilitators of SV fusion but are dispensable for "fusion clamping" in mammalian forebrain neurons.

INTRODUCTION

Synaptic vesicle (SV) fusion is executed by SNARE complexes, which force fusing membrane compartments into close proximity to overcome the energy barrier for fusion (Cohen and Melikyan, 2004; Jahn and Fasshauer, 2012; Jahn and Scheller, 2006; Südhof and Rothman, 2009). SNARE-mediated membrane fusion is intrinsically much slower than synaptic excitation-secretion coupling because the speed and fidelity of SV fusion is determined by a set of SNARE-interacting regulatory proteins (Südhof, 2014; Wojcik and Brose, 2007). Among these, complexins (Cplxs), evolutionarily conserved proteins that stoichiometrically bind SNARE complexes (Chen et al., 2002; McMahon et al., 1995; Zhou et al., 2017), are of eminent importance.

Mammals express four Cplx paralogs (Reim et al., 2001, 2005), of which Cplx1 is the predominant brain variant. Its expression largely overlaps with that of Cplx2 (Freeman and Morton, 2004), while Cplx3 is mainly and Cplx4 is exclusively found in retinal ribbon synapses (Reim et al., 2005). Homozygous Cplx2, Cplx3, or Cplx4 single-knockout (KO) mice and Cplx2/Cplx3 double-KO (DKO) mice are viable, while Cplx1 KO mice are ataxic, and Cplx1/Cplx2 DKO and Cplx1/Cplx2/Cplx3 triple-KO (TKO) mice die perinatally (Xue et al., 2008), indicating that Cplx1 has functions that cannot be fully compensated by its paralogs. At neuromuscular synapses of Cplx-KO *C. elegans* (Hobson et al., 2011; Wragg et al., 2013) and *Drosophila* (Huntwork and Littleton, 2007; Jorquera et al., 2012), evoked SV fusion is decreased, while spontaneous SV fusion is augmented, which led to the notion that Cplxs act as "fusion clamps" to inhibit spontaneous fusion. In mice, however, constitutive Cplx KO strongly attenuates SV fusion probability and thus reduces spontaneous and evoked fusion at conventional synapses (but see Mortensen et al., 2016), without affecting the number of fusion-competent SVs (Chang et al., 2015; Reim et al., 2001; Xue et al., 2008). This indicates that Cplxs facilitate SV fusion, possibly by maintaining SNARE complexes in a highly fusogenic state. Confirming data on Cplx KOs, experiments employing short hairpin RNA (shRNA)-mediated knockdown (KD) in cultured mammalian neurons (Yang et al., 2010, 2013) showed that acute Cplx KD reduces synaptic strength, but they also detected increases in spontaneous SV fusion rates, which are not seen in neurons of constitutive Cplx KOs (Reim et al., 2001; Xue et al., 2008). Furthermore, shRNA-mediated Cplx KD was reported to cause a decrease in the readily releasable pool of primed SVs (RRP) (Yang et al., 2013), which is not detectable in constitutive Cplx KOs (Reim et al., 2001; Xue et al., 2008).

Apart from possible species-related differences, the discrepant data on the role of Cplxs in SV fusion likely originate from the different perturbation methods used and the corresponding protein decay kinetics achieved. Indeed, in addition to a specifically altered SV fusion machinery, functional consequences of constitutive Cplx KO may reflect a combination of collateral perturbations, compensatory processes, or even aberrant synaptogenesis. Because acute and specific elimination of Cplx expression after synaptogenesis is required to distinguish between these possibilities, we generated a

Cplx1$^{flox/flox}$/Cplx2$^{-/-}$/Cplx3$^{-/-}$ conditional TKO (cTKO) mouse, which conditionally expresses Cplx1 as the sole Cplx isoform, and used it to assess the type, time course, and extent of functional changes upon acute genetic ablation of Cplx after synaptogenesis.

RESULTS

Generation of Cplx1$^{flox/flox}$ Mice

LoxP sites flanking exon 2 of the mouse *Cplx1* gene and a neomycin-resistance (Neo) cassette flanked by FRT sites were introduced into embryonic stem cells (129/ola) by homologous recombination (Augustin et al., 1999; Thomas and Capecchi, 1987) to generate Cplx1$^{Neo/+}$ mice. Cplx1$^{Neo/Neo}$ mice were crossed with FRT-overexpressing mice (Farley et al., 2000) to remove the Neo cassette and produce Cplx1$^{flox/flox}$ mice, which showed no obvious phenotypic changes. In parallel, Cplx1$^{Neo/Neo}$ mice were bred with EIIaCre deleter mice (Lakso et al., 1996) to delete *Cplx1* exon 2 and the Neo cassette. Like constitutive Cplx1 KO mice (Reim et al., 2001), the resulting Cplx1$^{cre/cre}$ mice were severely ataxic. Western blotting showed a loss of Cplx1 in Cplx1$^{cre/cre}$ mice. Cplx1$^{flox/flox}$ mice were crossed with Cplx2$^{-/-}$/Cplx3$^{-/-}$ DKO mice to generate cTKO mice for subsequent functional analyses, as cultured hippocampal Cplx2/Cplx3 DKO neurons have a wild-type (WT) phenotype and do not express Cplx4 (Reim et al., 2005; Xue et al., 2008) (Figures S1A–S1D).

Rapid Loss of Cplx1 upon Cre-Induced Recombination of the *Cplx1^{flox}* Locus

Cultured hippocampal neurons from P0 cTKO mice were allowed to establish synaptic networks (mass cultures) or autaptic connections (micro-island cultures) until day *in vitro* (div) 7, when they were infected with lentiviruses encoding RFP (Ctrl neurons/cultures) or RFP-Cre (Cre neurons/cultures) (day after infection [dai] 0). Uninfected cells served as additional controls for western blotting. Synaptic transmission was assessed between dai 3 (div 10) and dai 16 (div 23) (Figure 1A).

To assess the rate of Cplx1 loss after Cre infection, hippocampal mass cultures were analyzed using western blotting at dai 2–12, using tubulin as reference. Cplx1 levels in Ctrl neurons were unchanged with respect to those in uninfected cultures at all times tested. In Cre neurons, Cplx1 levels were unchanged at dai 2 (div 9), when most synapses had been formed, but then exponentially declined (τ = 2.8 days) (Figure 1B). Residual Cplx1 bands at dai $\geq$ 8 (<15% of Ctrl) are due to non-infected neurons. Accordingly, we observed a dramatic loss of anti-Cplx1/Cplx2 immunofluorescence in dai 8–9 Cre neurons, comparable with that in constitutive TKO cells, while the density and size of VGlut1-positive glutamatergic boutons along segments of primary dendrites were unchanged in Cre neurons (Figures S1E and S1F; Table S1). On the basis of these data, Cre-infected cTKO neurons at dai 8–16 can be regarded as Cplx deficient.

To assess the effects of Cplx loss on cell development, we measured passive membrane properties of mass-cultured Cre and Ctrl neurons (Mennerick et al., 1995). Unlike cortical but similar to olfactory neurons (Yang et al., 2013), mass-cultured Ctrl neurons showed a more pronounced developmental increase in membrane capacitance (C_m) than Cre neurons, so that the mean C_m was ~25% larger at dai 8–16 in Ctrl neurons, indicating a slight developmental retardation in the absence of Cplxs (Figure S1G; Table S1), which results in a smaller cell surface area.

Acute Cplx Loss Attenuates Spontaneous Glutamate and GABA Release in Mass Cultures

Pharmacologically isolated glutamatergic spontaneous miniature excitatory postsynaptic currents (mEPSCs) and GABAergic miniature inhibitory postsynaptic currents (mIPSCs) were recorded in hippocampal mass cultures at dai 3–16. All recordings were obtained at room temperature and with 2 mM Ca^{2+} and 2 mM Mg^{2+} in the bath. Because Cplx expression was completely abolished at dai $\geq$ 8 (Figure 1B), results obtained between dai 8 and dai 16 were pooled. For Cplx-deficient dai 8–16 Cre neurons, mean mEPSC and mIPSC rates were reduced to ~30% and ~18% of Ctrl values, while miniature postsynaptic current (mPSC) amplitudes and mPSC kinetics were unaffected (Figures 1C and 1D; Table S1). For early culture periods (dai 3–4), when Cplx levels in Cre neurons are $\geq$50% of Ctrl levels, average mPSC rates were similar, but they declined in Cre neurons for dai $\geq$ 4, when Cplx levels dropped below 50% of Ctrl levels (Figures 1B and 1E).

Acute Cplx Loss Reduces Spontaneous Glutamate Release and Synaptic Strength in Micro-Island Cultures

Because synaptogenesis in mass cultures is spatially unrestricted, neurons form a dense network that confounds the isolation of unitary evoked EPSCs (eEPSCs) and the interpretation of functional parameters. In contrast, neurons grown on glial micro-islands form synapses only with themselves (autapses) and can be easily activated and assayed (Bekkers and Stevens, 1991). We thus characterized action potential (AP)-evoked synaptic transmission using glutamatergic hippocampal autaptic cells. All analysis was restricted to infected neurons that were unequivocally identified on the basis of their RFP fluorescence.

mEPSC frequencies in autaptic Ctrl neurons were ~55% lower compared with mass cultures of similar age, likely because multiple presynaptic neurons converge onto individual neurons in the latter. As for mass cultures, mean mEPSC frequencies were similar in autaptic Cre and Ctrl neurons at dai 3–4 but were strongly reduced in Cre neurons (to 45% of Ctrl) at dai 8–16, with no effects on mEPSC amplitudes or kinetics (Figures S2A–S2C; Table S1).

Because spontaneous glutamate release is similarly reduced after acute Cplx KO in mass and micro-island cultures, we assessed AP-evoked autaptic eEPSCs in more detail. eEPSC amplitudes varied substantially (0.43–18.4 nA) in Ctrl neurons but were much smaller (0.046–1.8 nA) in Cre neurons (dai 8–16), with mean amplitudes reduced by ~88% (Figures 2A1 and 2B; Table S1). To estimate total release capacity Q_Σ (RRP), hyperosmotic solution was puff-applied, and the transient postsynaptic current response was integrated (Figure 2A2). Because quantal size (Q_{mEPSC}) was unchanged after Cplx loss (Figure S2B2; Table S1) and Q_Σ decreased only slightly at the latest developmental stages studied (Figures 2B and 2C3; Table S1),

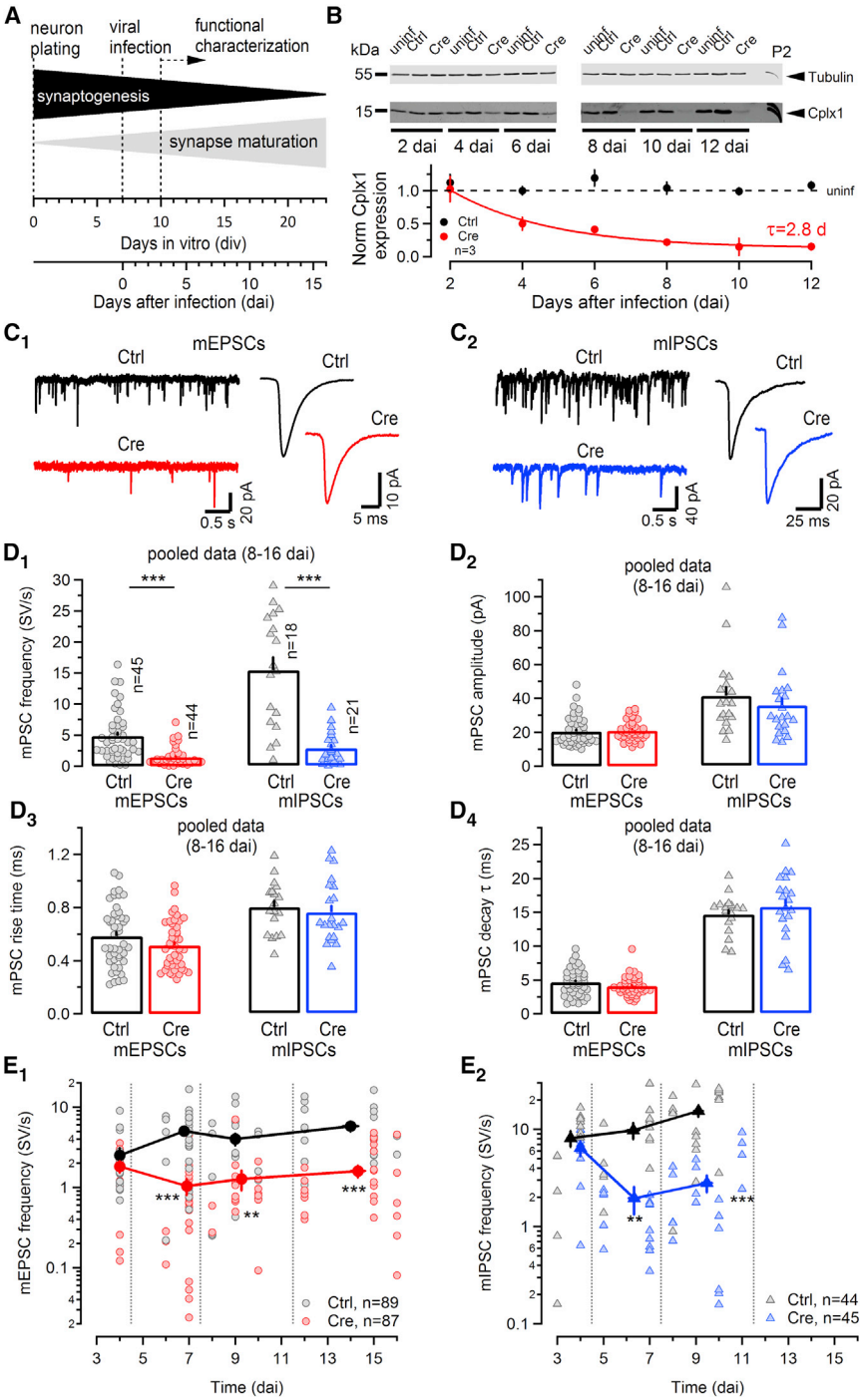

Figure 1. Acute Cplx Loss Causes Progressive Attenuation of Spontaneous Glutamate and GABA Release at Hippocampal Synapses in Mass Cultures

(A) P0–P1 hippocampal neurons from cTKO mice were maintained *in vitro* in mass cultures or on astrocyte micro-islands. At div 7, neurons were infected with either RFP (Ctrl) or Cre-RFP (Cre). Functional properties were assayed by patch-clamp recordings between dai 3 and dai 16 (div 10–23).

(B) Progressive loss of Cplx1 expression assayed by western blotting of mass cultures at dai 2, 4, 6, 8, 10, and 12. Cplx1 expression levels in RFP-infected Ctrl cultures were similar to uninfected cultures. Virtually complete loss of Cplx1 protein in Cre-infected cultures was observed at dai ≥ 8 (top). The time course of Cplx1 loss in Cre-infected cultures is well fit by an exponential function (τ = 2.8 days) (bottom, three biological replicates).

(C–E) Spontaneous SV fusion was characterized in mass cultures by recording spontaneously occurring mPSCs at dai 3–16. Glutamatergic mEPSCs and GABAergic mIPSCs were pharmacologically isolated by application of bicuculline (20 μM) and NBQX (2 μM) plus D-AP5 (40 μM), respectively. AP firing was suppressed by the addition of 0.5 μM TTX to the bath.

(C) Sample traces (left) and average waveforms (right) of mEPSCs (C1) and mIPSCs (C2) recorded in a Ctrl (black) and a Cre (red and blue) neuron at dai 10, when Cplx1 expression was completely abolished in Cre neurons.

(D) Pooled summary data for mPSC frequency (D1), amplitude (D2), and rise (D3) and decay (D4) kinetics for Ctrl (gray symbols) and Cre (red and blue symbols) neurons at dai 8–16.

(E) Scatterplots of frequency versus dai for mEPSCs (E1) and mIPSCs (E2) measured at dai 3–16. Pale symbols represent individual neurons; dark symbols and solid lines represent mean mPSC frequencies pooled for intervals dai 3–4, 5–7, 8–11, and ≥12.

Error bars represent SEM; **p < 0.01 and ***p < 0.001.

which is likely related to the smaller cell size and the concomitant decrease of the number of boutons per neuron at this stage (Figure S3C; Table S1), the smaller eEPSCs in Cre neurons were primarily caused by an ~5-fold drop in the average SV fraction released by single APs (*F*), from ~5% (Ctrl) to ~1% (Cre) (dai 8–16; Table S1). *F* was estimated as the average ratio of the early, synchronous eEPSC charge ($Q_{25\ ms}$, the charge transfer during the initial 25 ms after eEPSC onset) divided by Q_{Σ} for each individual cell. On the basis of our $Q_{25\ ms}$ and Q_{mEPSC} estimates, we conclude that the average number of synchronously released SVs per AP drops from ~207 (Ctrl) to ~31 (Cre) after acute Cplx KO (Table S1). Another *F* estimate was obtained from scatterplots of $Q_{25\ ms}$ versus Q_{Σ} (Figure 2D). For Ctrl eEPSCs, linear regression analysis shows that the relationship between these quantities is fit by a straight line passing through the origin, indicating similar *F* among Ctrl neurons, with larger eEPSCs primarily arising from larger Q_{Σ}. For Cre eEPSCs, the slope of the regression line was ~4.6-fold smaller. Finally, we found that Cplx loss does not affect RRP replenishment kinetics after sucrose-induced RRP depletion, indicating that Cplx is dispensable for SV priming (Figure S3D).

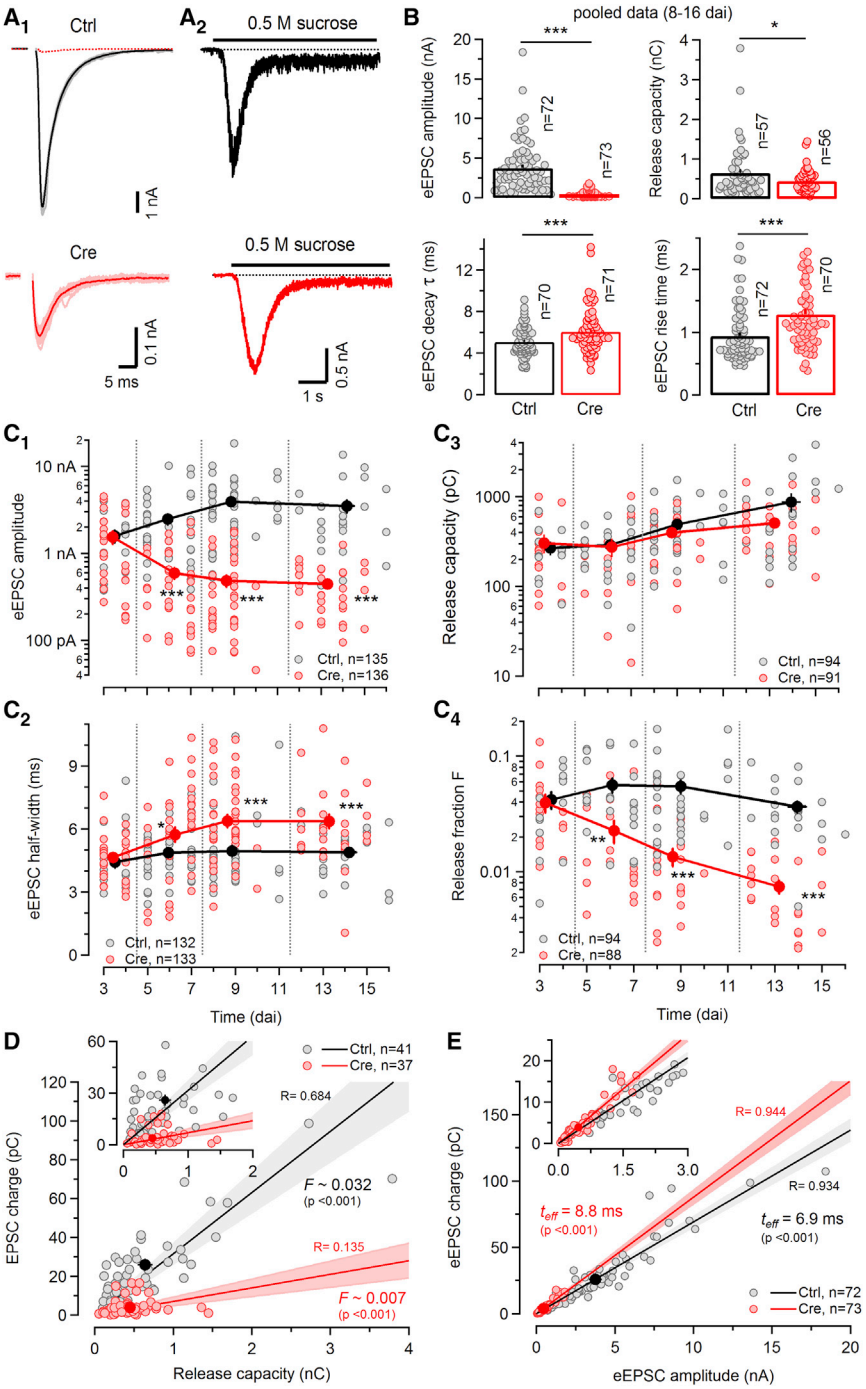

Figure 2. Acute Cplx Loss Causes Progressive Attenuation of Glutamatergic Synaptic Transmission in Autapses

(A) AP-evoked EPSCs (eEPSC) in dai 3–16 hippocampal neurons on glial micro-islands were elicited by brief somatic depolarization triggering escaping APs (1 ms, 0 mV). Light-colored traces represent 15 consecutive eEPSCs recorded at 5 s intervals in a Ctrl (day 9, gray) and a Cre (dai 11, rose) neuron. Voltage-gated Na^+ and K^+ currents are blanked for clarity. Average eEPSCs are superimposed in dark color (A1). The dotted red trace represents the average Cre eEPSC superimposed onto the Ctrl eEPSCs for comparison. (A2) Total release capacity (RRP) was probed by rapid application of hyperosmotic solution (0.5 Osm/L sucrose added to the bath solution). Traces in A2 show sucrose-triggered responses recorded in the same Cre (red) and Ctrl (black) neurons as in A1.

(B) Pooled summary data for eEPSC amplitudes (top left), release capacity (top right), and eEPSC decay (bottom left) and rise (bottom right) kinetics for Ctrl (black bars, gray symbols) and Cre (red bars and symbols) neurons at dai 8–16.

(C) Scatterplots of eEPSC amplitudes (C1), eEPSC half-widths (C2), release capacity (C3), and release fraction (C4) versus dai for eEPSCs recorded at dai 3–16. Pale symbols represent individual neurons; dark symbols and solid lines represent means of the respective parameters pooled for intervals dai 3–4, 5–7, 8–11, and ≥12.

(D) Scatterplot of eEPSC charges versus release capacities (RRP) for dai 8–16 autapses. Symbols represent individual Ctrl (gray) and Cre (red) neurons. Solid lines and shaded areas represent regression lines and 95% confidence intervals, respectively. The average release fraction *F* given by the slopes of the regression lines was significantly lower in Cre synapses.

(E) Scatterplot of eEPSC charges versus eEPSC amplitudes for dai 8–16 autapses. Symbols represent individual Ctrl (gray) and Cre (red) neurons. Solid lines and shaded areas represent regression lines and 95% confidence intervals, respectively. The "effective eEPSC duration" (t_{eff}) given by the slopes of the regression lines was prolonged in Cre neurons, consistent with their slower eEPSC kinetics.

Error bars represent SEM; shaded areas in (D) and (E) represent 95% confidence intervals; *p < 0.05, **p < 0.01, and ***p < 0.001.

As Cplx1 loss increases eEPSC duration in mouse calyx of Held synapses (Chang et al., 2015), we analyzed eEPSC waveforms in more detail and confirmed a slowing of rise and decay kinetics in Cre neurons (Figures 2B and 2C2). Because quantal event kinetics were unaltered, the slower eEPSC kinetics are consistent with less tightly synchronized AP-evoked SV fusion in Cre neurons. Linear regression analysis of scatterplots of eEPSC charge versus amplitude yielded larger slopes in Cre versus Ctrl neurons (Figure 2E), indicating that the "effective width" (t_{eff}) of eEPSCs (the width of a square current pulse with same amplitude as eEPSC peak and same integral as synchronous eEPSC charge $Q_{25\ ms}$) is prolonged in Cre neurons.

In a subset of dai 8–16 neurons, we determined the total number of VGlut1-positive puncta representing putative glutamatergic boutons per autaptic neuron. On the basis of mean values for release capacity and number of presynaptic boutons, we estimated an average *n* of ~12 SVs per bouton in Ctrl and Cre neurons (Table S1). These numbers agree well with the number of

morphologically docked SVs in hippocampal CA1 synapses in organotypic slices from WT and Cplx-deficient mice (Imig et al., 2014).

Assuming uniform release probability among boutons, we can estimate the probability of at least one SV being released by a single AP at a given bouton as $1 - (1 - F)^n$ (i.e., p = 0.446 and p = 0.114 for Ctrl and Cre neurons, respectively). Thus, during repeated synapse activation at intervals large enough to prevent RRP depletion, every 2.2th or every 8.8th AP releases at least one SV per synapse in Ctrl and Cre neurons, respectively. Neither eEPSC amplitudes and kinetics nor *F* differed at dai 3–4 (Figure 2C), but these parameters showed different developmental trends in Cre and Ctrl neurons for dai > 4.

In calyceal auditory glutamatergic synapses, delayed release measured after single eEPSCs or eEPSC trains is strongly augmented after Cplx loss (Chang et al., 2015; Strenzke et al., 2009), which was not seen in Cplx-KO hippocampal autaptic neurons (Reim et al., 2001). We quantified the number and relative fractions of SVs fusing synchronously and in a delayed manner in response to single APs (Figures S3A and S3B). For eEPSCs recorded at dai 3–4, the contribution of synchronous and delayed SV fusion to the total release amounted to a similar number of ~75 plus ~16 SVs and ~75 plus ~14 SVs (synchronous plus delayed SVs) in Ctrl and Cre neurons, respectively. In contrast, both release components were strongly and similarly reduced in dai 8–16 Cre neurons, with ~216 plus ~76 SVs and ~39 plus ~18 SVs in Ctrl and Cre neurons, respectively. Thus, the relative contribution of delayed SV fusion to total fusion following single APs remained nearly unchanged at ~25%. Of note, estimates for synchronously released SVs based on $Q_{25\ ms}$ or the fast component of double exponential fits to the cumulative eEPSC charge were very similar (e.g., 206 SVs versus 216 SVs for dai 8–16 Ctrl neurons).

Acute Cplx Loss Causes a Shift to Short-Term Facilitation and Delayed Transmitter Release in Response to AP Trains in Micro-Island Cultures

To assess changes in short-term synaptic plasticity in Cre neurons, we measured eEPSCs in response to 10 and 40 Hz AP trains. Ctrl eEPSC trains at dai 8–16 typically showed synaptic depression, presumably due to SV depletion, which was more pronounced at higher stimulation frequency (Figures 3A and 3B). In contrast, eEPSCs in Cre cells facilitated during trains, consistent with their lower initial *F* and consequently lower SV consumption rate. Because of the opposite changes in eEPSC amplitudes during trains, differences between Cre and Ctrl eEPSCs were less pronounced for late amplitudes ($eEPSC_{late}$ as the mean of $eEPSC_{13–15}$) than for initial amplitudes ($eEPSC_1$). Nevertheless, even $eEPSC_{late}$ amplitudes were reduced to ~27% (10 Hz) and ~44% (40 Hz) in Cre neurons, indicating that phasic and tonic transmission are severely impeded after acute Cplx KO. When grouping eEPSC trains according to dai, we noted that Cplx-expressing Cre neurons (dai 3–4) showed a Ctrl-like short-term plasticity pattern. Subsequently, synaptic depression decreased progressively in Ctrl neurons, consistent with a developmentally decreasing *F*. This developmental trend toward less depression was much more pronounced in Cre synapses and resulted in net facilitation of $eEPSC_{late}$ for 40 Hz trains, and even more so for 10 Hz stimulation, because of prevailing facilitation in the presence of weaker depression (Figure 3C).

We next analyzed delayed release following AP trains. Compared with Ctrl neurons, delayed SV fusion dropped in Cplx-deficient Cre neurons (dai 8–16) by ~55%–60% (Figure 3D; Table S1). Normalization of delayed release by the summed early release measured up to 50 ms after $eEPSC_{15}$ (up to 2.55 s [10 Hz] or 1.35 s [40 Hz] after the onset of stimulation) showed that its relative contribution increased in Cre neurons from ~9% to ~13% and from ~23% to ~29% for 10 and 40 Hz stimulation, respectively (dai 8–16) (Figure 3E). Thus, acute Cplx KO has two functional consequences for eEPSCs trains: a considerable decrease in the total amount of transmitter release and a shift from synchronous to delayed release. The finding that not only synchronous but also delayed transmitter release decreased substantially in hippocampal Cplx-deficient Cre autapses is in contrast to the situation at the calyx of Held synapses, where delayed release is augmented under the same conditions.

Acute Cplx Loss Reduces the Rates of All Modes of SV Fusion in Micro-Island Cultures

A key feature of presynaptic SV fusion is its highly non-linear sensitivity to $[Ca^{2+}]_i$, which causes rates of SV fusion to vary dramatically, from a few SV per second at resting $[Ca^{2+}]_i$ (<100 nM) to hundreds of SV per millisecond during AP-evoked transmitter release at several micromolar of $[Ca^{2+}]_i$ (Bollmann et al., 2000; Heidelberger et al., 1994; Schneggenburger and Neher, 2000). Because Cplx loss may differentially affect different forms of transmitter release, we assessed release rates in Cre and Ctrl neurons for four different synapse activation contexts, covering a range of SV fusion rates of ≥5 orders of magnitude: (1) spontaneous release, (2) asynchronous release in response to slightly elevated $[Ca^{2+}]_i$, (3) delayed release after AP trains, and (4) peak release during single APs (Figure 4).

To measure SV fusion rates in response to $[Ca^{2+}]_i$ elevated to a value similar to that typically reported for residual global $[Ca^{2+}]_i$ after AP firing (Lin et al., 2017; Müller et al., 2007), we dialyzed neurons with a pipette solution containing a Ca^{2+}-EGTA mixture with a nominal free $[Ca^{2+}]_i$ of ~1 μM (Lou et al., 2005) and recorded mEPSCs over 1 min periods every 2 min (Figure 4B). The final rates of asynchronous SV release were consistently lower in Cre neurons, with averages of ~35 versus ~9 SV/s for Ctrl versus Cre neurons (dai 8–16; Figures 4B3 and 4C). For comparison, we also estimated the release rates of delayed release after 10 and 40 Hz eEPSCs and found them to be reduced by ~54% (10 Hz) and ~44% (40 Hz) in Cre neurons (Figures 4A and 4C). Finally, we estimated peak release rates during AP-eEPSCs by dividing the maximum rate of eEPSC rise in each neuron by the respective mEPSC size. Consistent with the strongly reduced eEPSC peak amplitudes and slightly desynchronized time course of AP-evoked release in Cre neurons, we found an ~88% reduction in peak release rates in these neurons (Figure 4C). Together, these data demonstrate that for a wide range of SV fusion rates, from <10 SVs/s up to >100 SVs/ms, fusion rates are invariably reduced by 46%–88% upon acute Cplx loss.

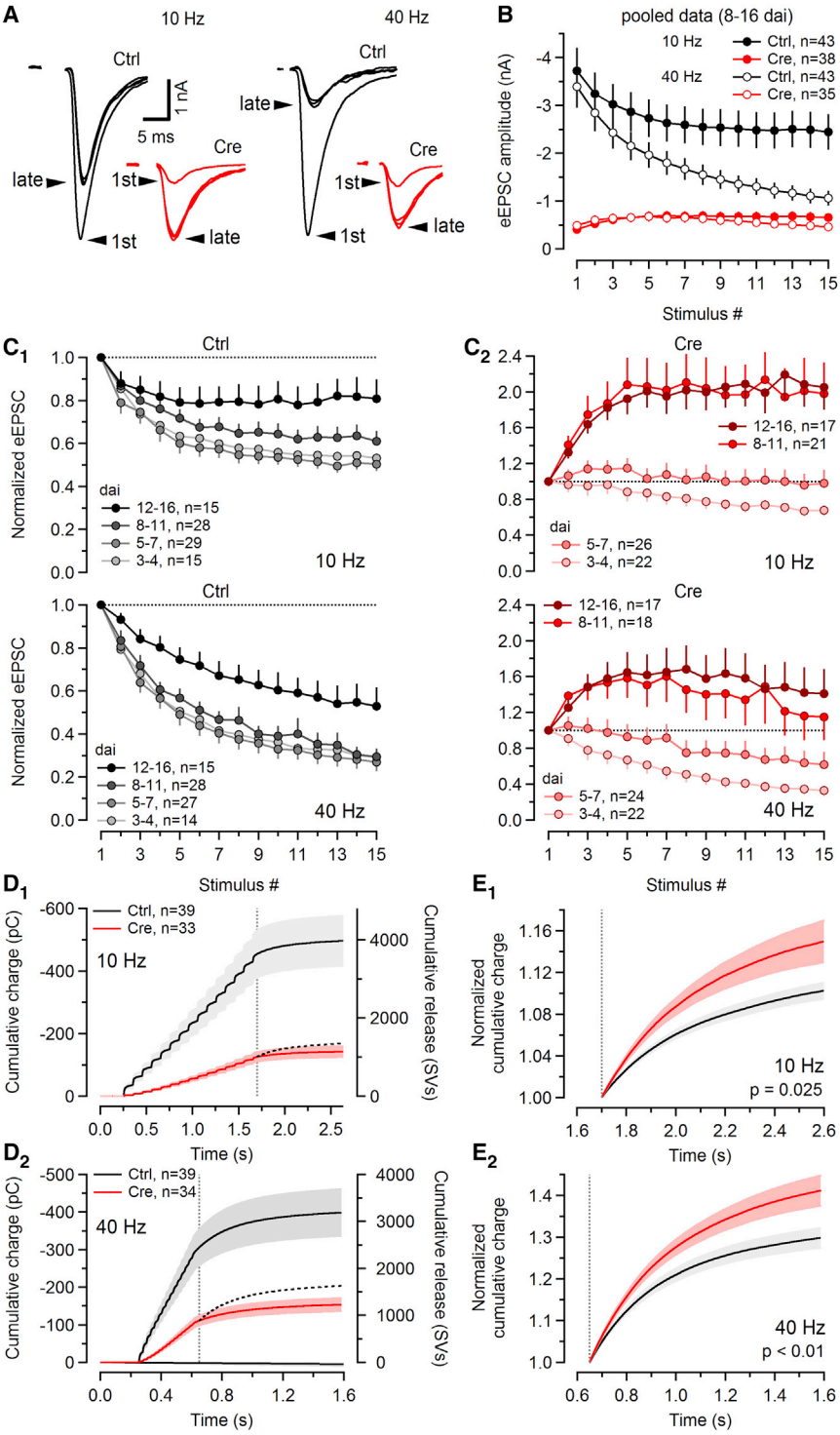

Figure 3. Acute Cplx Loss Causes a Progressive Shift of Short-Term Plasticity from Depression to Facilitation in Autapses

(A) Synaptic short-term plasticity was analyzed by recording eEPSCs in response to repetitive AP firing (15 APs). Initial EPSCs ($EPSC_1$, arrowheads labeled "1st") and late EPSCs ($EPSC_{13}$ to $EPSC_{15}$, arrowheads labeled "late") of trains are exemplified for a Ctrl (dai 10, black) and a Cre (dai 9, red) neuron stimulated at either 10 Hz (left) or 40 Hz (right). Voltage-gated Na^+ and K^+ currents are blanked for clarity.

(B) Summary of mean eEPSC amplitudes during train stimulation for 10 Hz (filled) and 40 Hz (empty) eEPSC trains recorded at dai 8–16 in Ctrl (black) and Cre cells (red).

(C) Short-term plasticity data grouped according to dai in Ctrl neurons (C1) and Cre neurons (C2) in response to 10 Hz (top) and 40 Hz (bottom) stimulation. eEPSC amplitudes were normalized to $eEPSC_1$.

(D) Delayed release was analyzed in dai 8–16 Ctrl (black) and Cre (red) neurons stimulated with 10 Hz (D1) and 40 Hz (D2) trains consisting of 15 APs. Cumulative eEPSC charges were plotted as a function of time (left). To separate delayed-release from early-release SVs, we assumed the onset of the former (dotted lines) to be 1.7 and 0.65 s after the onset of the eEPSC train for 10 Hz (D1) and 40 Hz (D2), respectively, corresponding to 50 ms after the onset of the last eEPSC in the trains ($\sim 10 \times \tau_{decay}$ of the eEPSC). The dotted black lines in D1 and D2 represent the delayed release component measured in Ctrl neurons, digitally added to the early release component measured in Cre neurons for comparison.

(E) Relative contribution of delayed release was compared by normalization to the total amount of early release measured 1.7 or 0.65 s after the onset of the eEPSC train for 10 Hz (E1) or 40 Hz (E2) stimulation.

Error bars and shaded areas in (D) and (E) represent SEM.

DISCUSSION

We generated a conditional Cplx1-KO mouse ($Cplx1^{flox/flox}$) to study functional consequences of Cplx1 loss in Cre-expressing neurons. By crossing $Cplx1^{flox/flox}$ mice into a Cplx2/Cplx3 DKO background, we obtained cTKO mice that lacked obvious abnormalities. We used these mice, which conditionally express Cplx1 as the sole Cplx isoform in the brain (except Cplx4 in retina), to study synaptic transmission in cultured hippocampal neurons, which require only Cplx1 for normal function (Xue et al., 2008). We let neurons grow *in vitro* until div 7 and then infected them with lentiviruses expressing Cre, which allowed us to study functional consequences of acute and complete genetic Cplx deletion at div $\geq$ 15 (i.e., dai $\geq$ 8), after synapse formation has peaked. Cplx1 expression is normal in uninfected cTKO neurons and identical to that in constitutive TKO neurons in Cre-infected cTKO neurons at dai $\geq$ 8. In this phase, Cre-induced Cplx deletion causes (1) a progressive reduction of mPSC frequencies, but

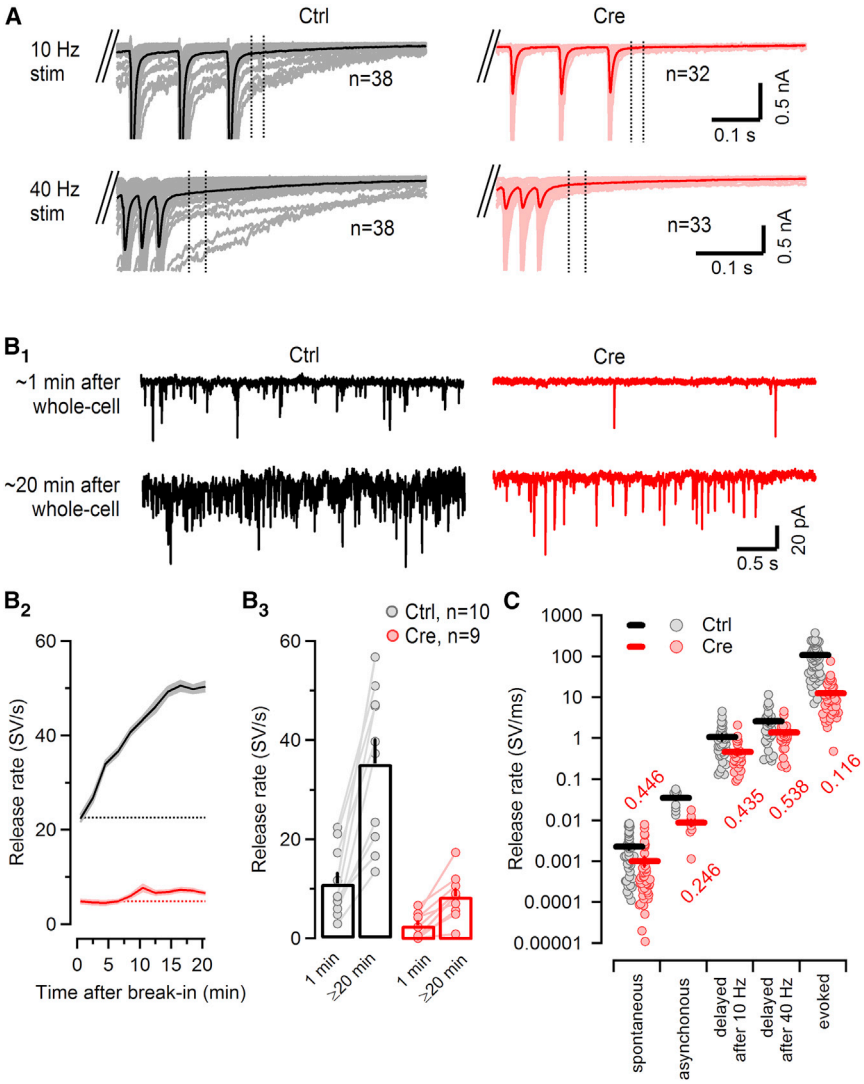

Figure 4. Acute Cplx Loss Causes Decreased Rates of Spontaneous, Asynchronous, Delayed, and Synchronous SV Fusion in Autapses

(A) Rates of delayed release after 10 Hz (top) or 40 Hz (bottom) eEPSC trains were estimated by dividing the average current amplitude measured during a 25 ms time window from 50–75 ms after the onset of the last eEPSC in the train by the corresponding charge of the mEPSC obtained in a given neuron. Light-colored traces represent individual cells. Dark-colored traces represent averages obtained from all neurons recorded.

(B) Asynchronous release assayed at hippocampal autaptic connections by dialysis with a buffered $[Ca^{2+}]_i$ solution. Ctrl (black) and Cre (red) neurons were dialyzed in whole-cell configuration with a pipette solution containing a nominal free $[Ca^{2+}]_i$ of ~1 μM. mEPSCs were recorded starting immediately after establishing whole-cell configuration up to 40 min. (B1) Sample traces recorded ~1 min (top) and ~20 min (bottom) after establishing whole-cell configuration. (B2) The rate of spontaneous SV fusion events increased gradually until reaching a plateau value in a time-dependent manner with a time course that presumably reflects the time course of diffusion of the elevated $[Ca^{2+}]_i$ from the tip of the patch-pipette to presynaptic release sites. (B3) The final asynchronous SV fusion rates were consistently lower in Cre neurons (right).

(C) Summary data comparing release rate estimates for spontaneous, asynchronous, delayed, and evoked glutamate release in Ctrl (black) and Cre (red) neurons in hippocampal micro-island cultures. Estimated release rates under the experimental conditions tested covered a range of ≥5 orders of magnitude. Cre neurons consistently showed lower release rates compared with Ctrl neurons under all experimental conditions. Fractions given in red represent $rate_{Cre}/rate_{Ctrl}$ ratios.

Shaded areas in (B2) and error bars in (B3) represent SEM.

not kinetics and amplitudes, at glutamatergic and GABAergic synapses; (2) strongly reduced synaptic strength as assessed by autaptic AP-eEPSCs, due mainly to an ~5-fold reduced release fraction *F*; (3) less synchronized glutamate release, causing slower eEPSC kinetics; (4) facilitation of glutamate release during AP trains, consistent with a lower *F*; and (5) reduction of the absolute, but not the relative, contribution of delayed glutamate release to total release following short AP trains.

$Cplx1^{flox/flox}$ mice were validated by a set of western blotting experiments demonstrating that brain Cplx1 expression was unchanged between WT and $Cplx1^{flox/flox}$ mice and equally abolished in brains of constitutive Cplx1-KO and $Cplx1^{flox/flox}$ mice after crossing with EIIaCre deleter mice. These findings show that the $Cplx1^{flox/flox}$ allele functions normally and validate the penetrance of the Cre-recombined $Cplx1^{flox/flox}$ KO allele. Analyses of mass-cultured neurons showed that Cplx1 expression in uninfected cTKO neurons and in neurons infected with RFP- or Cre-RFP-expressing viruses is identical shortly after infection (dai 2). It then decreases progressively in Cre cultures, as assessed by western blotting, and at the cellular level to the expression levels seen in constitutive TKO cells, as assessed by immunostaining. These findings are consistent with the fact that Cre neurons do not show any functional deficits at dai 1–4 but later, when Cplx expression levels drop below 50% of control (dai ≥ 8), develop defects that ultimately phenocopy those in constitutively Cplx-deficient neurons. The observed exponential time course of Cplx1 loss in Cre cultures ($\tau = 2.8$ days) indicates a Cplx1 half-life of $t_{½} = \tau \times \ln(2) = 1.94$ days, which matches the estimated half-life of rat Cplx1 in cultured cortical neurons, as assessed by pulse-chase isotope labeling (1.78 days; Heo et al., 2018).

In agreement with previous studies on constitutive KOs (Chang et al., 2015; Reim et al., 2001; Xue et al., 2007) but in contrast to findings obtained with an shRNA KD approach (Yang et al., 2013), we found that acute Cplx loss leaves RRP size and replenishment kinetics unaffected (Chang et al.,

2015). These findings show that Cplxs are not required for SV docking and priming (Imig et al., 2014).

In contrast to its attenuation of evoked transmitter release, acute shRNA KD of Cplx was reported to augment spontaneous SV fusion (Yang et al., 2013). However, KD-induced augmentation of spontaneous release was even observed in Cplx1/Cplx2 DKO neurons in the same study, indicating the possibility of an off-target effect. We compared spontaneous transmitter release, multiple forms of Ca^{2+}-evoked asynchronous release in response to elevated $[Ca^{2+}]_i$, and AP-evoked release between Ctrl and Cre neurons and invariably found that the rate of SV fusion is lower after acute Cplx KO. Moreover, mPSC frequencies decreased continuously with progressive loss of Cplx, indicating that there is no intermediate phase during Cplx loss when spontaneous fusion transiently increases. Finally, we assayed in one paradigm transmitter release in response to dialysis of neurons with elevated $[Ca^{2+}]_i$ via the recording pipette, thus circumventing presynaptic voltage-gated Ca^{2+} channel opening and also observed reduced SV fusion rates in Cplx KO cells. In accord with studies on Cplx-deficient calyx of Held terminals, in which presynaptic Ca^{2+} currents are unaffected after Cplx loss (Chang et al., 2015), these data indicate that the reduced transmitter release rates in Cplx KO neurons are not due to aberrant Ca^{2+} influx.

Overall, our data indicate that Cplxs are strong SV fusion-promoting factors that act upon SNARE complexes to increase the fusion propensity of SVs (Trimbuch and Rosenmund, 2016). Our data are incompatible with a role of Cplx as a "fusion clamp." It is currently still unclear why Cplx loss increases spontaneous SV fusion in some instances (Mortensen et al., 2016). Assuming that a substantial fraction of spontaneous SV fusion events are Ca^{2+} dependent, it is possible that Cplx-deficient SNARE complexes differ from Cplx-bound ones in their affinity for the Ca^{2+} sensors involved in spontaneous SV fusion (e.g., synaptotagmins and/or DOC2s) (Courtney et al., 2018; Groffen et al., 2010; Xu et al., 2009). For instance, a shift of Cplx-free SNARE complexes toward preferred interactions with the high-affinity Ca^{2+} sensor DOC2 or related C2 domain-containing proteins could explain increased mPSC rates upon Cplx loss in certain contexts. In addition, different resting Ca^{2+} concentrations or the absence of additional regulators of spontaneous SV fusion, such as the actin cytoskeleton (Morales et al., 2000), might explain why certain synapses respond to Cplx loss with increased spontaneous SV fusion. Finally, it is possible that the increased spontaneous SV fusion rate upon constitutive Cplx loss that is seen in certain synapse types is a consequence of partially aberrant synapse formation.

STAR★METHODS

Detailed methods are provided in the online version of this paper and include the following:

- KEY RESOURCES TABLE
- CONTACT FOR REAGENT AND RESOURCE SHARING
- EXPERIMENTAL MODEL AND SUBJECT DETAILS
  - Generation of $Cplx1^{flox/flox}Cplx2^{-/-}Cplx3^{-/-}$ mice
  - Mouse maintenance
- METHOD DETAILS
  - Neuronal cultures
  - DNA constructs, generation of lentiviruses, and viral infection
  - Western blot analysis
  - Immunocytochemistry
  - Electrophysiological recordings
- QUANTIFICATION AND STATISTICAL ANALYSIS
  - Offline analysis
  - Image analysis
  - Statistical analysis

SUPPLEMENTAL INFORMATION

Supplemental Information can be found with this article online at https://doi.org/10.1016/j.celrep.2019.02.030.

ACKNOWLEDGMENTS

This work was supported by the German Research Foundation (FZT 103 to N.B. and H.T.), the European Commission (ERC AdG "Synprime" to N.B.), and an Alexander von Humboldt Foundation postdoctoral fellowship (F.J.L.-M.). We thank J.-S. Rhee for discussions and sharing equipment, E. Neher for discussions and advice regarding data analysis, N. Lipstein and T. López-Hernández for valuable feedback, A. Günther for preparing astrocyte cultures, and F. Benseler, the AGCT Laboratory, and T. Hellmann for excellent technical assistance.

AUTHOR CONTRIBUTIONS

N.B. and K.R. conceived the original idea. K.R. generated and validated the conditional Cplx1 KO. F.J.L.-M. and H.T. designed electrophysiological experiments. F.J.L.-M. performed electrophysiological recordings and immunohistochemical experiments and prepared all figures. F.J.L.-M. and H.T. analyzed and interpreted electrophysiological data. O.J. performed biochemical analysis. F.J.L.-M., N.B., and H.T. wrote the paper. K.R. provided conceptual feedback and manuscript edits. All authors read and approved the final manuscript.

DECLARATION OF INTERESTS

The authors declare no competing interests.

Received: June 26, 2018
Revised: September 5, 2018
Accepted: February 7, 2019
Published: March 5, 2019

REFERENCES

Augustin, I., Rosenmund, C., Südhof, T.C., and Brose, N. (1999). Munc13-1 is essential for fusion competence of glutamatergic synaptic vesicles. Nature *400*, 457–461.

Bekkers, J.M., and Stevens, C.F. (1991). Excitatory and inhibitory autaptic currents in isolated hippocampal neurons maintained in cell culture. Proc. Natl. Acad. Sci. U S A *88*, 7834–7838.

Bollmann, J.H., Sakmann, B., and Borst, J.G. (2000). Calcium sensitivity of glutamate release in a calyx-type terminal. Science *289*, 953–957.

Burgalossi, A., Jung, S., Man, K.N., Nair, R., Jockusch, W.J., Wojcik, S.M., Brose, N., and Rhee, J.S. (2012). Analysis of neurotransmitter release mechanisms by photolysis of caged Ca^{2+} in an autaptic neuron culture system. Nat. Protoc. *7*, 1351–1365.

Chang, S., Reim, K., Pedersen, M., Neher, E., Brose, N., and Taschenberger, H. (2015). Complexin stabilizes newly primed synaptic vesicles and prevents

their premature fusion at the mouse calyx of held synapse. J. Neurosci. *35*, 8272–8290.

Chen, X., Tomchick, D.R., Kovrigin, E., Araç, D., Machius, M., Südhof, T.C., and Rizo, J. (2002). Three-dimensional structure of the complexin/SNARE complex. Neuron *33*, 397–409.

Clements, J.D., and Bekkers, J.M. (1997). Detection of spontaneous synaptic events with an optimally scaled template. Biophys. J. *73*, 220–229.

Cohen, F.S., and Melikyan, G.B. (2004). The energetics of membrane fusion from binding, through hemifusion, pore formation, and pore enlargement. J. Membr. Biol. *199*, 1–14.

Courtney, N.A., Briguglio, J.S., Bradberry, M.M., Greer, C., and Chapman, E.R. (2018). Excitatory and inhibitory neurons utilize different Ca^{2+} sensors and sources to regulate spontaneous release. Neuron *98*, 977–991.e5.

Farley, F.W., Soriano, P., Steffen, L.S., and Dymecki, S.M. (2000). Widespread recombinase expression using FLPeR (flipper) mice. Genesis *28*, 106–110.

Fesce, R. (1990). Stochastic approaches to the study of synaptic function. Prog. Neurobiol. *35*, 85–133.

Freeman, W., and Morton, A.J. (2004). Differential messenger RNA expression of complexins in mouse brain. Brain Res. Bull. *63*, 33–44.

Goda, Y., and Stevens, C.F. (1994). Two components of transmitter release at a central synapse. Proc. Natl. Acad. Sci. U S A *91*, 12942–12946.

Groffen, A.J., Martens, S., Díez Arazola, R., Cornelisse, L.N., Lozovaya, N., de Jong, A.P., Goriounova, N.A., Habets, R.L., Takai, Y., Borst, J.G., et al. (2010). Doc2b is a high-affinity Ca2+ sensor for spontaneous neurotransmitter release. Science *327*, 1614–1618.

Heidelberger, R., Heinemann, C., Neher, E., and Matthews, G. (1994). Calcium dependence of the rate of exocytosis in a synaptic terminal. Nature *371*, 513–515.

Heo, S., Diering, G.H., Na, C.H., Nirujogi, R.S., Bachman, J.L., Pandey, A., and Huganir, R.L. (2018). Identification of long-lived synaptic proteins by proteomic analysis of synaptosome protein turnover. Proc. Natl. Acad. Sci. U S A *115*, E3827–E3836.

Hobson, R.J., Liu, Q., Watanabe, S., and Jorgensen, E.M. (2011). Complexin maintains vesicles in the primed state in C. elegans. Curr. Biol. *21*, 106–113.

Hooper, M., Hardy, K., Handyside, A., Hunter, S., and Monk, M. (1987). HPRT-deficient (Lesch-Nyhan) mouse embryos derived from germline colonization by cultured cells. Nature *326*, 292–295.

Hsia, H.E., Kumar, R., Luca, R., Takeda, M., Courchet, J., Nakashima, J., Wu, S., Goebbels, S., An, W., Eickholt, B.J., et al. (2014). Ubiquitin E3 ligase Nedd4-1 acts as a downstream target of PI3K/PTEN-mTORC1 signaling to promote neurite growth. Proc. Natl. Acad. Sci. U S A *111*, 13205–13210.

Huntwork, S., and Littleton, J.T. (2007). A complexin fusion clamp regulates spontaneous neurotransmitter release and synaptic growth. Nat. Neurosci. *10*, 1235–1237.

Imig, C., Min, S.W., Krinner, S., Arancillo, M., Rosenmund, C., Südhof, T.C., Rhee, J., Brose, N., and Cooper, B.H. (2014). The morphological and molecular nature of synaptic vesicle priming at presynaptic active zones. Neuron *84*, 416–431.

Jahn, R., and Fasshauer, D. (2012). Molecular machines governing exocytosis of synaptic vesicles. Nature *490*, 201–207.

Jahn, R., and Scheller, R.H. (2006). SNAREs—engines for membrane fusion. Nat. Rev. Mol. Cell Biol. *7*, 631–643.

Jones, D.H., and Matus, A.I. (1974). Isolation of synaptic plasma membrane from brain by combined flotation-sedimentation density gradient centrifugation. Biochim. Biophys. Acta *356*, 276–287.

Jorquera, R.A., Huntwork-Rodriguez, S., Akbergenova, Y., Cho, R.W., and Littleton, J.T. (2012). Complexin controls spontaneous and evoked neurotransmitter release by regulating the timing and properties of synaptotagmin activity. J. Neurosci. *32*, 18234–18245.

Laemmli, U.K. (1970). Cleavage of structural proteins during the assembly of the head of bacteriophage T4. Nature *227*, 680–685.

Lakso, M., Pichel, J.G., Gorman, J.R., Sauer, B., Okamoto, Y., Lee, E., Alt, F.W., and Westphal, H. (1996). Efficient in vivo manipulation of mouse genomic sequences at the zygote stage. Proc. Natl. Acad. Sci. U S A *93*, 5860–5865.

Lin, K.H., Taschenberger, H., and Neher, E. (2017). Dynamics of volume-averaged intracellular Ca^{2+} in a rat CNS nerve terminal during single and repetitive voltage-clamp depolarizations. J. Physiol. *595*, 3219–3236.

Liu, P., Jenkins, N.A., and Copeland, N.G. (2003). A highly efficient recombineering-based method for generating conditional knockout mutations. Genome Res. *13*, 476–484.

Lou, X., Scheuss, V., and Schneggenburger, R. (2005). Allosteric modulation of the presynaptic Ca^{2+} sensor for vesicle fusion. Nature *435*, 497–501.

Malagon, G., Miki, T., Llano, I., Neher, E., and Marty, A. (2016). Counting vesicular release events reveals binomial release statistics at single glutamatergic synapses. J. Neurosci. *36*, 4010–4025.

McMahon, H.T., Missler, M., Li, C., and Südhof, T.C. (1995). Complexins: cytosolic proteins that regulate SNAP receptor function. Cell *83*, 111–119.

Mennerick, S., Que, J., Benz, A., and Zorumski, C.F. (1995). Passive and synaptic properties of hippocampal neurons grown in microcultures and in mass cultures. J. Neurophysiol. *73*, 320–332.

Morales, M., Colicos, M.A., and Goda, Y. (2000). Actin-dependent regulation of neurotransmitter release at central synapses. Neuron *27*, 539–550.

Mortensen, L.S., Park, S.J.H., Ke, J.B., Cooper, B.H., Zhang, L., Imig, C., Löwel, S., Reim, K., Brose, N., Demb, J.B., et al. (2016). Complexin 3 increases the fidelity of signaling in a retinal circuit by regulating exocytosis at ribbon synapses. Cell Rep. *15*, 2239–2250.

Müller, M., Felmy, F., Schwaller, B., and Schneggenburger, R. (2007). Parvalbumin is a mobile presynaptic Ca^{2+} buffer in the calyx of Held that accelerates the decay of Ca^{2+} and short-term facilitation. J. Neurosci. *27*, 2261–2271.

Naldini, L., Blömer, U., Gallay, P., Ory, D., Mulligan, R., Gage, F.H., Verma, I.M., and Trono, D. (1996). In vivo gene delivery and stable transduction of nondividing cells by a lentiviral vector. Science *272*, 263–267.

Neher, E., and Sakaba, T. (2003). Combining deconvolution and fluctuation analysis to determine quantal parameters and release rates. J. Neurosci. Methods *130*, 143–157.

Pernía-Andrade, A.J., Goswami, S.P., Stickler, Y., Fröbe, U., Schlögl, A., and Jonas, P. (2012). A deconvolution-based method with high sensitivity and temporal resolution for detection of spontaneous synaptic currents in vitro and in vivo. Biophys. J. *103*, 1429–1439.

Reim, K., Mansour, M., Varoqueaux, F., McMahon, H.T., Südhof, T.C., Brose, N., and Rosenmund, C. (2001). Complexins regulate a late step in Ca^{2+}-dependent neurotransmitter release. Cell *104*, 71–81.

Reim, K., Wegmeyer, H., Brandstätter, J.H., Xue, M., Rosenmund, C., Dresbach, T., Hofmann, K., and Brose, N. (2005). Structurally and functionally unique complexins at retinal ribbon synapses. J. Cell Biol. *169*, 669–680.

Schneggenburger, R., and Neher, E. (2000). Intracellular calcium dependence of transmitter release rates at a fast central synapse. Nature *406*, 889–893.

Segal, J.R., Ceccarelli, B., Fesce, R., and Hurlbut, W.P. (1985). Miniature endplate potential frequency and amplitude determined by an extension of Campbell's theorem. Biophys. J. *47*, 183–202.

Strenzke, N., Chanda, S., Kopp-Scheinpflug, C., Khimich, D., Reim, K., Bulankina, A.V., Neef, A., Wolf, F., Brose, N., Xu-Friedman, M.A., and Moser, T. (2009). Complexin-I is required for high-fidelity transmission at the endbulb of Held auditory synapse. J. Neurosci. *29*, 7991–8004.

Südhof, T.C. (2014). The molecular machinery of neurotransmitter release (Nobel lecture). Angew. Chem. Int. Ed. Engl. *53*, 12696–12717.

Südhof, T.C., and Rothman, J.E. (2009). Membrane fusion: grappling with SNARE and SM proteins. Science *323*, 474–477.

Thomas, K.R., and Capecchi, M.R. (1987). Site-directed mutagenesis by gene targeting in mouse embryo-derived stem cells. Cell *51*, 503–512.

Towbin, H., Staehelin, T., and Gordon, J. (1979). Electrophoretic transfer of proteins from polyacrylamide gels to nitrocellulose sheets: procedure and some applications. Proc. Natl. Acad. Sci. U S A *76*, 4350–4354.

Trimbuch, T., and Rosenmund, C. (2016). Should I stop or should I go? The role of complexin in neurotransmitter release. Nat. Rev. Neurosci. *17*, 118–125.

Wojcik, S.M., and Brose, N. (2007). Regulation of membrane fusion in synaptic excitation-secretion coupling: speed and accuracy matter. Neuron *55*, 11–24.

Wragg, R.T., Snead, D., Dong, Y., Ramlall, T.F., Menon, I., Bai, J., Eliezer, D., and Dittman, J.S. (2013). Synaptic vesicles position complexin to block spontaneous fusion. Neuron *77*, 323–334.

Xu, J., Pang, Z.P., Shin, O.H., and Südhof, T.C. (2009). Synaptotagmin-1 functions as a Ca2+ sensor for spontaneous release. Nat. Neurosci. *12*, 759–766.

Xue, M., Reim, K., Chen, X., Chao, H.T., Deng, H., Rizo, J., Brose, N., and Rosenmund, C. (2007). Distinct domains of complexin I differentially regulate neurotransmitter release. Nat. Struct. Mol. Biol. *14*, 949–958.

Xue, M., Stradomska, A., Chen, H., Brose, N., Zhang, W., Rosenmund, C., and Reim, K. (2008). Complexins facilitate neurotransmitter release at excitatory and inhibitory synapses in mammalian central nervous system. Proc. Natl. Acad. Sci. U S A *105*, 7875–7880.

Yang, X., Kaeser-Woo, Y.J., Pang, Z.P., Xu, W., and Südhof, T.C. (2010). Complexin clamps asynchronous release by blocking a secondary Ca(2+) sensor via its accessory α helix. Neuron *68*, 907–920.

Yang, X., Cao, P., and Südhof, T.C. (2013). Deconstructing complexin function in activating and clamping Ca^{2+}-triggered exocytosis by comparing knockout and knockdown phenotypes. Proc. Natl. Acad. Sci. U S A *110*, 20777–20782.

Zhou, Q., Zhou, P., Wang, A.L., Wu, D., Zhao, M., Südhof, T.C., and Brunger, A.T. (2017). The primed SNARE-complexin-synaptotagmin complex for neuronal exocytosis. Nature *548*, 420–425.

STAR★METHODS

KEY RESOURCES TABLE

REAGENT or RESOURCE	SOURCE	IDENTIFIER
Antibodies		
Rabbit polyclonal anti-Cplx1,2	Synaptic Systems	Cat# 122002; RRID: AB_122002
Rabbit polyclonal anti-Tubulin	SIGMA	Cat# T3526; RRID: AB_261659
Guinea-Pig polyclonal anti-VGluT1	Synaptic Systems	Cat# 135304; RRID: AB_135304
IRDye800 goat-anti-rabbit secondary antibody	LI-COR	Cat# 926-32211; RRID: AB_621843
Alexa Fluor 488 goat-anti-rabbit secondary antibody	Thermo Fischer	Cat# A11008; RRID: AB_A11008
Cy5.5 goat-anti-guinea pig secondary antibody	Novus Biologicals	Cat# NB120-6967; RRID: AB_NB120-6967
Bacterial and Virus Strains		
f(syn)w-iCreRFP-P2Alang	Prof. Christian Rosenmund lab	N/A
BL-f(syn)w-NLS-RFP-P2Alang	Prof. Christian Rosenmund lab	N/A
Biological Samples		
Mouse hippocampi from Cplx1$^{flox/flox}$/Cplx2$^{-/-}$/Cplx3$^{-/-}$ (cTKO) mice (neuronal cultures)	This paper	N/A
Mouse cortici from C57BL/6JRj mice (astrocyte feeding layers)	Janvier Labs	N/A
Chemicals, Peptides, and Recombinant Proteins		
Tetrodotoxin citrate	Alomone Labs	Cat#T-550; RRID: SCR_013570
NBQX disodium salt	HelloBio	HB0443
Bicuculline methiodide	HelloBio	HB0893
D-AP5	Tocris	Cat#0106; RRID: SCR_003689
Experimental Models: Cell Lines		
Mouse: 129/ola embryonic stem cell line E14	Hooper et al., 1987	N/A
Experimental Models: Organisms/Strains		
Mouse: Cplx1$^{flox/flox}$	This paper	N/A
Mouse: Cplx1$^{cre/cre}$	This paper	N/A
Mouse: Cplx1$^{flox/flox}$/Cplx2$^{-/-}$/Cplx3$^{-/-}$ (cTKO)	This paper	N/A
Mouse: CaMKII–Cre–159 [Tg(Camk2a-cre)159Kln]	Lakso et al., 1996	N/A
Mouse: FLPeR (R26^{Fkt})	Farley et al., 2000	N/A
Mouse: C57BL/6JRj	Janvier Labs	N/A
Oligonucleotides		
Cplx1 Neo sense primer 5′-CGCTTGAGGAGGCTGGCG-3′	This paper	N/A
Cplx1 Neo antisense primer 5′-CCCAGCCAAACCAACAGT-3′	This paper	N/A
Cplx1 floxed sense primer 5′-GGCACGAAAACACATGGCTG-3′	This paper	N/A
Cplx1 floxed antisense primer 5′-CAGTGGGTTCCACTGCACC-3′	This paper	N/A
Recombinant DNA		
Plasmid: pBlueMG-CPX10A	Reim et al., 2001	N/A
Plasmid: pBlueMG-CPX10B	Reim et al., 2001	N/A
Plasmid: PL253	Liu et al., 2003	N/A
Plasmid: PL452	Liu et al., 2003	N/A
Plasmid: PL451	Liu et al., 2003	N/A
Software and Algorithms		
ImageStudioLite	LI-COR	http://www.licor.com RRID:SCR_013715
Patch Master v2x53	HEKA/Harvard Bioscience	http://www.heka.com RRID:SCR_000034

(*Continued on next page*)

Continued

REAGENT or RESOURCE	SOURCE	IDENTIFIER
IgorPro 6.3.7.2	Wavemetrics	http://www.wavemetrics.com RRID:SCR_000325
LCS SP2	Leica Microsystems	http://www.leica-microsystems.com RRID:SCR_008960
ImageJ 1.50i	National Institute of Health	https://imagej.nih.gov RRID:SCR_003070
Microsoft Office Excel 2010	Microsoft	https://www.microsoft.com RRID:SCR_016137
R 3.5.1	The R foundation	http://www.r-project.org RRID:SCR_001905

CONTACT FOR REAGENT AND RESOURCE SHARING

Further information can be obtained from and requests for reagents may be directed to and will be fulfilled by the Lead Contact, Nils Brose (brose@em.mpg.de).

EXPERIMENTAL MODEL AND SUBJECT DETAILS

Generation of Cplx1$^{flox/flox}$Cplx2$^{-/-}$Cplx3$^{-/-}$ mice

Mice with a floxed exon 2 of the *Cplx1* gene were generated by homologous recombination in embryonic stem cells (ES). The conditional KO vector contained DNA fragments of two genomic clones (pBlueMG-CPX10A and pBlueMG-CPX10B; Reim et al., 2001). Using recombineering (Liu et al., 2003), two loxP sites were introduced, 212 bp upstream of exon 2 (representing bp 72-175 of the Cplx1 cDNA, GenBank accession number NM_007756) and 53 bp downstream of the Neomycin resistance cassette, which was flanked by two FRT sites. The vector also contained a thymidine kinase gene (Figure S1A). After electroporation of 129/ola ES cells and selection by using Ganciclovir and G418 (Thomas and Capecchi, 1987), resistant ES cell clones were analyzed by Southern blotting of HindIII-digested genomic DNA (Figure S1B). Positive clones were injected into blastocysts to obtain chimeric mice that transmitted the mutation through the germline. Germline transmission was confirmed by PCR (Cplx1 Neo sense primer 5′-CGCTTGAG GAGGCTGGCG-3′, Cplx1 Neo antisense primer 5′-CCCAGCCAAACCAACAGT-3′). Mice homozygous for the recombined Cplx1 locus were bred with mice overexpressing FRT recombinase (Farley et al., 2000), by which the Neo cassette was removed (Figure S1A). Genotyping of DNA from tail biopsies was done by PCR (Cplx1 floxed sense primer 5′-GGCACGAAAACACATGGCTG-3′, Cplx1 floxed antisense primer 5′-CAGTGGGTTCCACTGCACC-3′) (Figure S1C). Mice homozygous for this mutation (Cplx1$^{flox/flox}$) were crossed into Cplx2/Cplx3 DKO animals, resulting in Cplx1$^{flox/flox}$/Cplx2$^{-/-}$/Cplx3$^{-/-}$ (cTKO) mice. These, and in addition in some cases corresponding control animals (Cplx1$^{WT/WT}$/Cplx2$^{-/-}$/Cplx3$^{-/-}$), were used for further analyses. In parallel, mice homozygous for the initial recombined Cplx1 locus were bred with EIIaCre deleter mice (Lakso et al., 1996), which resulted in the loss of exon 2 of mouse *Cplx1* and the removal of the Neo cassette (Figure S1A). Routine genotyping of litters of those breedings was performed by PCR using the Cplx1 Neo sense and the Cplx1 floxed antisense primers (Figure S1C).

Mouse maintenance

All animal experiments were in compliance with the applicable animal care guidelines and performed as approved by the Lower Saxony State Office for Consumer Protection and Food Safety (LAVES; permits 33.9-42502-04-13/1359 and 33.19-42502-04-15/1921). Animals were maintained in groups in accordance with European Union Directive 63/2010/EU and ETS 123 (individually ventilated cages, specific pathogen-free conditions, 21 ± 1°C, 55% relative humidity, 12 h/12 h light/dark cycle). Mice received food and tap water *ad libitum* and were provided with bedding and nesting material. Cages were changed once a week. Animal health was controlled daily by caretakers and by a veterinarian. Health monitoring (serological analyses; microbiological, parasitological, and pathological examinations) was done quarterly according to FELASA recommendations with either NMRI sentinel mice or animals from the colony. The mouse colony used for experiments did not show signs of pathogens. The sex of animals used for experimentation was not checked because all previous studies on Cplx KOs had indicated that the sex does not affect the Cplx KO phenotype of cultured neurons.

METHOD DETAILS

Neuronal cultures

Hippocampal neurons derived from P0 cTKO mice irrespective of their sex were maintained *in vitro* in mass culture or on glial microislands. Cultures were used for electrophysiological characterization, immunofluorescence, and western blot analysis between div 10 and 23. Micro-island cultures were prepared as described previously (Burgalossi et al., 2012). Astrocytes used for glial feeder layers were obtained from cortices dissected from postnatal day (P) 0–1 WT mice and enzymatically digested for 15 min at 37°C with

0.25% (w/v) trypsin-EDTA solution (GIBCO). Astrocytes were cultured for 7–10 days in T75 flasks in DMEM (GIBCO) containing 10% FBS and penicillin (100 U/ml)/streptomycin (100 μg/ml). Subsequently, astrocytes were trypsinized and plated at a density of ~30,000 cells per coverslip onto 32 mm-diameter glass coverslips that were first coated with agarose (Sigma), and subsequently stamped using a custom-made stamp with a solution containing poly-D-lysine (Sigma-Aldrich), acetic acid, and collagen (BD Biosciences) to generate 400 × 400 μm^2 substrate islands permitting astrocyte attachment and growth. Hippocampi from cTKO P0 mice were isolated and digested for 55 min at 37°C in DMEM containing 2.5 U/ml papain (Worthington Biomedical Corp.), 0.2 mg/ml cysteine (Sigma), 1 mM $CaCl_2$, and 0.5 mM EDTA. After washing, dissociated neurons were seeded onto micro-island plates in serum-free Neurobasal medium (GIBCO) supplemented with B27 (GIBCO), Glutamax (GIBCO), and penicillin/streptomycin (100 U/ml, 100 μg/ml) at a density of ~4,500 neurons per 32 mm coverslip. Only islands containing single neurons were further analyzed. Mass cultures of hippocampal neurons were prepared as described above, except that dissociated hippocampal neurons were seeded in the same serum-free Neurobasal medium onto 18 mm-diameter glass coverslips coated with poly-D-Lysine (two hippocampi per 12-well plate). For mass cultures, the culture medium was replaced completely one day after plating, and partially thereafter once a week.

DNA constructs, generation of lentiviruses, and viral infection

Expression vectors encoding lentiviral supplementary proteins (pCMVdeltaR8.2 and VSV-G) and the pFUGW expression vector were described previously (Hsia et al., 2014). A f(syn)-ugw vector kindly provided by C. Rosenmund (Charité, Berlin, Germany) allowed us to produce two classes of lentiviruses: RFP-expressing and Cre × RFP-expressing viruses, which both induced nuclear expression of monomeric red fluorescence protein (mRFP) that served as an infection marker. Lentiviruses were generated as previously described (Naldini et al., 1996). HEK293FT cells (GIBCO, Germany; R700–07; RRID:CVCL_6911) plated on a poly-L-lysine (Sigma) coated 15 cm plastic dish were transfected with the packaging pVSV-G, the envelope pCMVdeltaR8.2, and the backbone vectors, either f(syn)w-NLS-RFP-P2Alang or f(syn)w-iCreRFP-P2Alang using Lipofectamine 2000 (Invitrogen, USA) according to the manufacturer's instructions. Cells were incubated with the transfection mix for 6 h in Opti-MEM (GIBCO) containing 10% fetal bovine serum (FBS, GIBCO). The medium was subsequently changed to DMEM (GIBCO) containing 2% FBS, 10 units/mL penicillin (GIBCO), 10 μg/mL streptomycin (GIBCO), and 10 mM sodium butyrate (Merck). Forty-eight hours after transfection, the culture medium containing lentiviral particles was harvested and concentrated using Amicon particle centrifugal filters (100 kDa, Millipore, USA). High-titer lentiviral samples were aliquoted, snap-frozen in liquid N_2, and stored at −80°C until used. HEK293FT cells used for virus production were obtained from a low passage culture (P3) from the original cell line purchased from GIBCO and checked for mycoplasma every 6 months. Neurons were infected at div 7, designated as day after infection (dai) 0. RFP fluorescence was checked at an excitation wavelength of 540 nm. RFP-positive neurons could be clearly detected at dai ≥ 3 (div ≥ 10). Based on the fraction of neurons with RFP-positive nuclei among all cells, we estimated that ~95 % of neurons in mass culture were typically infected (Ctrl: 95.8 ± 0.2 % of a total of 523 ± 26 cells per image, Cre: 95.7 ± 0.4 % of a total of 518 ± 43 cells per image, n = 6 images per group [3.2 mm^2 per image] derived from 2 different cultures). In micro-island cultures, the fraction of infected neurons was nearly 100% because RFP-negative neurons were never encountered after viral infection.

Western blot analysis

Crude synaptosomes were prepared as described (Jones and Matus, 1974). SDS-PAGE and immunoblotting were performed using standard procedures (Laemmli, 1970; Towbin et al., 1979). Primary antibodies for western blotting were a rabbit polyclonal anti-Cplx1,2 (1:4000; Synaptic Systems, RRID:AB_122002) and a rabbit polyclonal anti-Tubulin (1:20000; SIGMA, RRID:AB_261659) antibody. Immunoreactive proteins were detected by using an IRDye800 goat-anti-rabbit secondary antibody (1:5000; LI-COR, RRID:AB_621843) and visualized with the Odyssey® Near-Infrared System (LI-COR).

Immunocytochemistry

Neurons were fixed with 4% paraformaldehyde (w/v) in phosphate-buffered saline (PBS, pH 7.4), for 15–20 min. Following three washes with PBS, cells were permeabilized for 30 min using 0.3% (v/v) Triton X-100 in PBS while applying gentle agitation before being transferred into a solution containing 0.1% (v/v) Triton X-100, 20% (v/v) normal goat serum (GIBCO), and 0.2% (w/v) fish skin gelatin (Sigma) in PBS to block non-specific antibody binding (1.5 h). The same solution was used for diluting primary and secondary antibodies, except that normal goat serum concentration was lowered to 1% (v/v). Neurons were incubated with primary antibodies overnight at 4°C, followed by incubation with fluorophore-conjugated secondary antibodies for 2 h at room temperature (RT). After repetitive washes with PBS, coverslips were mounted using Aqua-Poly/Mount medium (Polysciences Inc.). Primary antibodies were a rabbit polyclonal anti-Cplx1,2 (1:1000; Synaptic Systems, RRID:AB_122002) and a guinea pig polyclonal anti-VGluT1 antibody (1:1000; Synaptic Systems, RRID:AB_135304). Secondary antibodies were a goat anti-rabbit Alexa Fluor 488 (Thermo Fischer; RRID: AB_A11008) and a goat anti-guinea pig Cy5.5 antibody (Novus Biologicals; RRID: AB_NB120-6967).

Electrophysiological recordings

Patch-clamp recordings were obtained at RT exclusively from infected neurons that were unequivocally identified by their RFP-positive nuclei. Neurons were whole-cell voltage-clamped at a holding potential (V_h) of −70 mV using an EPC10 amplifier controlled by Patchmaster or Pulse software (HEKA). Sampling intervals and low-pass filter settings were 20 μs and 5.0 kHz, respectively.

Patch-pipettes were pulled from borosilicate glass capillaries with filament (Science Products) on a P-97 Flaming/Brown Puller (Sutter Instruments) to have an open-tip resistance of 3–5 MΩ when filled with a pipette solution containing (in mM) 136 KCl, 17.5 HEPES, 1 EGTA, 0.6 $MgCl_2$, 4 $MgATP_2$, 0.3 $MgGTP_2$, 15 creatine phosphate, and 5 U/ml phosphocreatine kinase (~320 mOsmol/l, pH 7.4). The extracellular bath solution contained (in mM) 140 NaCl, 2.4 KCl, 10 HEPES, 2 $CaCl_2$, 2 $MgCl_2$, 10 D-glucose (~320 mOsmol/l, pH 7.3). Spontaneous miniature postsynaptic currents (mPSCs) in mass cultures were recorded in the presence of 0.5 μM TTX to block AP firing. TTX was absent when mPSCs were recorded in micro-island cultures because only islands hosting single neurons were used for voltage-clamp. Glutamatergic mEPSCs and GABAergic mIPSCs were pharmacologically isolated by adding 2 μM NBQX/40 μM D-AP5 and 20 μM bicucullin, respectively, to the bath solution. Seven out of 25 Ctrl neurons were excluded from the mIPSC analysis because their average rates were > 30 Hz and could not be reliably estimated. Consequently, the reported mean mIPSC frequency of Ctrl neurons represents an underestimate. Since they continued to increase during the entire culture period, we did not attempt to quantify mIPSC rates in mass-cultured Ctrl neurons beyond dai 11. Single AP-evoked autaptic EPSCs (eEPSCs) were induced by brief depolarizations (1 ms to −10 mV from V_h = −70 mV), triggering escaping APs. Mean eEPSC waveforms were obtained by averaging 10 consecutive sweeps recorded at an interval ≥ 5 s. eEPSC trains were recorded in response to 10 Hz and 40 Hz trains consisting of 15 APs. eEPSC train amplitudes represent averages of ≥ 3 consecutive sweeps recorded every 15 s. The release capacity (RRP) was determined by applying hyperosmotic solution (0.5 Osm/l sucrose added to the bath solution) for 6 s and quantified by integrating the transient component of the sucrose-evoked eEPSCs (typically lasting ~2–3 s) without correction for SV pool replenishment. Drug and sucrose solutions were gravity fed and applied via a valve-controlled fast perfusion system (SF-77B, Warner Instruments). All chemicals were from Sigma, except TTX (Alomone Labs), bicucullin (HelloBio), NBQX (HelloBio), and D-AP5 (Tocris). Passive membrane capacitance transients elicited by brief depolarization (from V_h = −70 to −60 mV for 30 ms, 10 repetitions) were recorded in mass-cultured hippocampal neurons and analyzed offline to estimate their membrane surface area. To quantify asynchronous release rates induced by elevated internal Ca^{2+} concentration ($[Ca^{2+}]_i$), neurons were permeabilized via the patch pipette with a solution containing (in mM) 92.05 K-gluconate, 20 KCl, 20 EGTA, 19 $CaCl_2$, 0.6 $MgCl_2$, 0.3 NaGTP, 4 NaATP (~337 mOsmol/l, pH 7.3, nominal free $[Ca^{2+}]$ ~1 μM calculated by MAXCHELATOR software). Every 2 min, spontaneously occurring mEPSCs were continuously recorded for a period of 60 s, starting 1 min after establishing whole-cell configuration and up to 20–40 min. During this time, we observed a substantial progressive increase in the mEPSC frequency with a time-course presumably reflecting the diffusion of the elevated $[Ca^{2+}]_i$ from the pipette to presynaptic release sites (Figure 4B2). Since the final mEPSC rates in control neurons frequently exceeded the maximum rate for reliable release event detection via a sliding template algorithm (1/30 ms = 33 s^{-1} see below), we estimated the asynchronous release rates in these experiments from the variance of band-pass filtered current traces using the mean mEPSC time course for calibration (Neher and Sakaba, 2003; Segal et al., 1985). The latter was established by averaging events that were extracted during the initial recording period when the release rate was still relatively low (≤23 s^{-1}).

QUANTIFICATION AND STATISTICAL ANALYSIS

Offline analysis

All offline analysis of electrophysiological data was performed in Igor Pro (Wavemetrics). Recordings were offset corrected and low-pass filtered with a cut-off frequency f_c = 3 kHz using a 10-pole digital Bessel filter. For the majority of mPSCs recordings, spontaneously occurring events were detected in continuous current sweeps by applying a sliding template-based detection algorithm (Clements and Bekkers, 1997). Event detection templates had a length of 30 ms or 50 ms for identifying either mEPSCs or mIPSCs, respectively, which allowed for a reliable detection of non-overlapping events occurring at maximum frequencies of 1/30 ms = 33 s^{-1} or 1/50 ms = 20 s^{-1}. Because mIPSCs recorded in mass cultures often occurred in bursts of events that periodically exceeded a rate of 20 s^{-1}, a deconvolution-based detection algorithm (Malagon et al., 2016; Pernía-Andrade et al., 2012) was preferred for analysis. Both detection algorithms yielded identical results when mIPSCs occurred at a low rate. Kinetic parameters determining the template waveform were established for each cell from the average of a family of visually identified events. Peak eEPSCs release rates were derived by dividing the fastest rate of eEPSC rise by the quantal size. The former was approximated by the ratio of 0.2 × eEPSC peak amplitude over the 40%–60% eEPSC rise time. Because this approach may underestimate the peak rate of eEPSC rise and does not take into account the finite rise time of quantal events, our peak eEPSC release rates represent a lower estimate. Rates of delayed release after eEPSC trains were derived by dividing the mean eEPSC amplitude measured during a 25 ms time window from 50–75 ms after the onset of the last eEPSC ($eEPSC_{15}$) by the quantal charge. Assuming an exponentially decaying rate of delayed release and considering that the late eEPSC current component decayed ~50–70 times more slowly than the mEPSCs decay, this method only slightly overestimates the rates of delayed release by a factor of $1/\left(1-\frac{\tau_q}{\tau_r}\right)$ (Goda and Stevens, 1994); where τ_q and τ_r are the exponential decay time constants of the mEPSC and the rate of delayed release, respectively), which equates to ~1.02. Asynchronous release rates for recordings in which cells were dialyzed with elevated $[Ca^{2+}]_i$ were estimated from postsynaptic current fluctuations. According to Campbell's theorem, the 2nd cumulant of the current fluctuations (variance) is proportional to the rate of statistically independent random events and can be expressed as $\lambda_2 = r \times h^2 \times \int [F(t)]^2 dt$, where λ_2 is the 2nd cumulant of the current fluctuations, r the rate, h the amplitude and $F(t)$ the time course of the random events (Fesce, 1990;

Neher and Sakaba, 2003). Errors arising from slow, spurious changes in membrane potential or high frequency whole-cell noise unrelated to transmitter release can be minimized by analyzing band-pass filtered recordings, such that the mEPSC rate is estimated by $r = (\lambda'_2 - \lambda'_{2,0})/((1 + CV^2) \times h^2 \times \int [F'(t)]^2 dt)$, where $\lambda'_{2,0}$ and λ'_2 are the respective background and release-associated variances of fluctuations of the band-pass filtered postsynaptic current, and $F'(t)$ is the time course of the mEPSC waveform after band-pass filtering. $\lambda'_{2,0}$ was estimated from current stretches lacking visually identifiable events. The term $1+CV^2$ corrects for the amplitude dispersion of mEPSCs (Segal et al., 1985) and was established by analyzing spontaneously occurring mEPSC recorded under control conditions (normal $[Ca^{2+}]_i$). *CV* was assumed to be 0.6 for all recordings. The digital band-pass filter consisted of a single-pole high-pass filter (f_c = 10 Hz) followed by a Gaussian low-pass filter (f_c = 1 kHz) and largely preserved the asymmetry of the mEPSC waveform. Numbers and relative fractions of SVs fusing synchronously and in a delayed manner in response to single APs were quantified by integrating EPSCs and fitting the cumulative eEPSC charges with a double exponential function $Q_s \times (1 - \exp(-(t - t_0)/\tau_s)) + Q_d \times (1 - \exp(-(t - t_0)/\tau_d))$, where Q_s and Q_d are amplitudes and τ_s and τ_d are time constants of postsynaptic charge components arising from synchronous and delayed release, respectively, and t_0 is the onset of the response. Because exponential fitting produced sometimes unreliable Q_d estimates, especially for small and noisy cumulative eEPSC charges obtained in Cre neurons, the magnitude of delayed release was estimated by subtracting the amplitude of the fast (synchronous) charge component Q_s from the total charge measured 225 ms after the onset of the eEPSC ($Q_{225\ ms}$). Because delayed release decayed slowly with a time constant of ~150–250 ms and had not ceased completely after 225 ms, our Q_d represents a lower estimate. Postsynaptic current integrals were converted to the equivalent number of SVs by assuming an mEPSC charge of 0.125 pC. Error estimates were obtained by bootstrap analysis using 1000 bootstrap samples. To analyze the magnitude of delayed release following AP trains, we separated delayed from early transmitter release by considering the sum of all SVs fusing $\geq$ 50 ms (~10 × τ_{decay} of mEPSCs) after the onset of the last eEPSC of the trains ($eEPSC_{15}$) as delayed. Because asynchronous release builds up already during the stimulus train, this approach underestimates the total asynchronous release. The rate constant of SV pool replenishment was estimated by recording a train of 15 eEPSCs (0.2 Hz) following application of a depleting sucrose (6 s, 0.5 Osm/l) pulse. Assuming a first order kinetic scheme for SV release and replenishment, we note that the inverse of the time constant ($1/\tau$) with which the fractions of empty and occupied SV docking sites relax to their new equilibrium values is determined by the sum of the two rate constants determining release (r) and replenishment (k), $^1/_\tau = k + r$. With $r = p \times f$, where p is SV fusion probability and f is the stimulation frequency, we obtain an estimate for k as $^1/_\tau - p \times f$. Membrane capacitance estimates of mass-cultured hippocampal neurons were obtained by analyzing capacitive current transients recorded in response to 10 mV depolarizations using a simplified two-compartment equivalent circuit model (Mennerick et al., 1995). Mean current transients obtained by averaging 10 consecutive sweeps were fitted using a double-exponential function $I(t) = A_1 \times e^{-t/\tau_1} + A_2 \times e^{-t/\tau_2} + A_\infty$, where $I(t)$ is the amplitude of the current at time t, A_1 and τ_1 denote the amplitude and time constant of the fast component of decay, A_2 and τ_2 represent the amplitude and time constant of the slower component of decay, and A_∞, is the difference between the holding current and the final steady-state current at the end of the depolarizing pulse. Estimates for proximal (C_{prox}) and distal (C_{dist}) cell capacitance, presumably representing the capacitance of soma plus proximal dendrites and distal dendrites, respectively, were obtained from these parameters as detailed elsewhere (Mennerick et al., 1995).

Image analysis

Images were acquired with a Leica SP2 confocal microscope at high magnification (40 × objective, NA 1.25; 63 × objective, NA 1.40) using a resolution of 1024 × 1024 pixels, corresponding to a pixel size of 0.37 × 0.37 μm^2 (40 ×) and 0.094 × 0.094 μm^2 (63 ×). Horizontal image planes in stacks were separated by ~0.3 μm resulting in $\geq$ 1 cross-sections trough individual synaptic boutons. Image analysis was carried out using ImageJ (NIH). Putative glutamatergic presynaptic boutons were identified in maximum intensity projections of anti-VGluT1 fluorescence image stacks. VGluT1 fluorescence levels were converted to binary using an appropriate threshold, and VGluT1-positive puncta were identified using the particle-analysis algorithm implemented in ImageJ by restricting their size to 0.1–2.0 μm^2. Identified puncta were stored as regions of interest (ROIs) and used to quantify intensities of anti-Cplx1,2 and anti-VGluT1 fluorescence in glutamatergic boutons. Synapse density was estimated either by counting the number of putative boutons along 50 μm long segments of primary dendrites (mass cultures) or by counting total synapse number over the entire cell surface area (micro-island cultures).

Statistical analysis

Data are expressed as mean ± standard error of the mean (SEM). Error bars in all graphs indicate SEM. Unless indicated otherwise, n refers to the number of cells tested (Table S1, Figures 1, 2, 3, and 4, Figures S1–S3). The total number of cultures was 20. Because the sample distribution of many parameters was skewed and non-Gaussian, statistical significance of differences in sample location was tested with two-tailed permutation tests using $\geq$ 10,000 random permutations. Statistical analysis was carried out in R (R Foundation for Statistical Computing). One, two, and three stars in figure panels indicate statistically significant differences at $p < 0.05$, $p < 0.01$ and $p < 0.001$, respectively.